4830 *Chem. Mater.* **2009,** *21,* 4830–4838
DOI:10.1021/cm901095v

CHEMISTRY OF MATERIALS
Article

Neutron Diffraction Studies of Nickel-Containing Perovskite Oxide Catalysts Exposed to Autothermal Reforming Environments

Jennifer R. Mawdsley,* John T. Vaughey, and Theodore R. Krause

Chemical Sciences & Engineering Division, Argonne National Laboratory, Argonne, Illinois 60439

Received April 21, 2009. Revised Manuscript Received September 1, 2009

Six nickel-containing perovskite oxides ($La_{1-x}Sr_x)M_{0.9}Ni_{0.1}O_{3\pm\delta}$, where $x = 0$ or 0.2 and M = Cr, Fe, or Mn) were used to catalyze the autothermal reforming of isooctane (C_8H_{18}) into a hydrogen-rich gas during short-term tests at 700 °C. To determine the phase stability of the samples in the reducing environment of the reforming reactor, characterization studies of the as-prepared and tested perovskite samples were conducted using powder X-ray diffraction, powder neutron diffraction, transmission electron microscopy, and scanning electron microscopy. We determined that the reducing conditions of the microreactor caused metallic nickel to form in all six compositions. However, the extent of the nickel loss from the perovskite lattices varied: the chromium-containing compositions lost the least nickel, compared to the manganese- and iron-containing compositions, and the strontium-free compositions lost more nickel than their strontium-containing analogs. Five of the six perovskite compositions tested showed no breakdown of the perovskite lattice despite the loss of nickel from the B-sites, producing only the third example of a B-cation-deficient, 3d transition-metal-containing perovskite.

1. Introduction

Catalytic autothermal reforming (ATR) of hydrocarbon fuels to produce hydrogen[1] has been proposed as one way to produce hydrogen at distributed locations, such as vehicle refueling stations. Hydrogen produced in this manner could be used for fuel-cell-powered vehicles or for stationary power generation systems until the technical difficulties associated with safely and economically storing and transporting pure hydrogen from centralized plants are overcome. In the ATR process, a hydrocarbon fuel, water, and oxygen, usually in the form of air, are reacted in the presence of a catalyst to generate a hydrogen-rich gas, which can be fed to a fuel cell as reformate, or treated further to produce pure hydrogen. The principal advantage of ATR over other catalytic processes, such as steam reforming or partial oxidation, is a more rapid and controlled response to the transient conditions[2,3] that might be experienced at a hydrogen refueling station. Another advantage of ATR over steam reforming is that ATR reactors would require smaller footprints, because of the fact that the heat required for the endothermic steam reforming reaction is supplied by the simultaneous exothermic partial oxidation reaction within the reactor vessel. A smaller footprint would be important at urban locations.

Perovskite oxides that contain rare earths and first-row transition metals, often doped with alkaline-earth metals, have been widely investigated as catalysts for a variety of applications, including methane combustion, methane steam reforming, partial oxidation and complete oxidation of various hydrocarbon fuels and alcohols, three-way catalysis, and ATR of liquid fuels used in transportation.[4−18] Perovskite oxides have the general formula ABO_3, where A is a lanthanide or alkaline-earth metal and B is a transition metal. Both the A and B cations can be partially substituted with different cations ($A_{1-x}A'_xB_{1-y}B'_yO_{3\pm\delta}$) to introduce structural and electronic defects which may enhance catalytic performance.

*Author to whom correspondence should be addressed. E-mail: mawdsley@anl.gov.

(1) Kumar, R.; Ahmed, S.; Krumpelt, M.; Myles, K. Fuel Cell System for Transportation Applications, U.S. Patent 5,248,566, Sept. 28, **1993**.
(2) Ahmed, S.; Krumpelt, M. *Int. J. Hydrogen Energy* **2001**, *26*, 291–301.
(3) Krumpelt, M.; Krause, T. R.; Carter, J. D.; Kopasz, J. P.; Ahmed, S. *Catal. Today* **2002**, *77*, 3–16.
(4) Doshi, R.; Alcock, C. B.; Gunasekaran, N.; Carberry, J. J. *J. Catal.* **1993**, *140*, 557–563.
(5) Arai, H.; Yamada, T.; Eguchi, K.; Seiyama, T. *Appl. Catal.* **1986**, *26*, 265–276.
(6) McCarty, J. G.; Wise, H. *Catal. Today* **1990**, *8*, 231–248.
(7) Choudhary, V. R.; Uphade, B. S.; Belhekar, A. A. *J. Catal.* **1996**, *163*, 312–318.
(8) Liu, D. J.; Krumpelt, M. *Int. J. Appl. Ceram. Technol.* **2005**, *2*, 301–307.
(9) Mawdsley, J. R.; Krause, T. R. *Appl. Catal., A* **2008**, *334*, 311–320.
(10) Qi, A. D.; Wang, S. D.; Fu, G. Z.; Ni, C. J.; Wu, D. Y. *Appl. Catal., A* **2005**, *281*, 233–246.
(11) Seiyama, T. *Catal. Rev.—Sci. Eng.* **1992**, *34*, 281–300.
(12) Sfeir, J.; Buffat, P. A.; Möckli, P.; Xanthopoulos, N.; Vasquez, R.; Mathieu, H. J.; Van herle, J.; Thampi, K. R. *J. Catal.* **2001**, *202*, 229–244.
(13) Stojanovic, M.; Mims, C. A.; Moudallal, H.; Yang, Y. L.; Jacobson, A. J. *J. Catal.* **1997**, *166*, 324–332.
(14) Valderrama, G.; Goldwasser, M. R.; Urbina de Navarro, C.; Tatibouët, J. M.; Barrault, J.; Batiot-Dupeyrat, C.; Martínez, F. *Catal. Today* **2005**, *107−108*, 785–971.
(15) Yamazoe, N.; Teraoka, Y. *Catal. Today* **1990**, *8*, 175–199.
(16) Dinka, P.; Mukasyan, A. S. *J. Power Sources* **2007**, *167*, 472–481.
(17) Sauvet, A. L.; Fouletier, J.; Gaillard, F.; Primet, M. *J. Catal.* **2002**, *209*, 25–34.
(18) Zhou, K. B.; Chen, H. D.; Tian, Q.; Hao, Z. P.; Shen, D. X.; Xu, sX. B. *J. Mol. Catal A: Chem.* **2002**, *189*, 225–232.

 Published on Web 10/02/2009

For the oxidation reactions, cation B is believed to be responsible for the catalytic activity while cation A is considered to be responsible for stabilizing the oxidation state of cation B.[15,19] The oxidation activity of perovskites has been attributed to mixed electronic and ionic conductivity, the presence of oxygen-ion vacancies, and the mobility of oxygen within the lattice[4]—characteristics that are believed to enhance the catalytic performance of other ceramic catalyst supports, such as doped-cerium oxide.[20,21] Our interest in pursuing perovskites as catalysts is due to the fact that as these materials do not require precious metals, they have the potential to be less expensive than noble metals supported on an oxide substrate.

A previous study that we conducted on nickel-based perovskite ATR catalysts[9] raised questions about their phase stability in the reducing conditions of the reactor, in particular, whether the nickel remains in the perovskite structure. In this study, we have evaluated the ATR catalytic performance of perovskite oxides of the general formula $La_{1-x}Sr_xM_{0.9}Ni_{0.1}O_{3\pm\delta}$, where $x = 0$ or 0.2, and M = Cr, Mn, or Fe. We also investigated the stability of our samples using X-ray diffraction (XRD) and neutron diffraction. Neutron diffraction offers the advantage of being particularly sensitive to nickel, because nickel has one of the largest neutron scattering lengths of all of the elements, so that even small amounts can be easily detected.[22] The fuel used in our ATR tests of the perovskites was isooctane (2,2,4-trimethylpentane). The objectives of this study were to determine (i) how composition affects catalytic performance, and (ii) if the various compositions are crystallographically stable under the reducing environment of ATR, i.e., whether metallic nickel forms on these catalysts.

2. Experimental Section

2.1. Catalyst Preparation. The perovskite catalysts were synthesized using the self-combusting glycine−nitrate process.[23] Solutions were prepared from the respective nitrates of each element (>99% pure, Aldrich), and the concentration of each solution was determined gravimetrically by thermal decomposition to the oxide or, in some cases, by inductively coupled plasma−optical emission spectroscopy (ICP-OES). The prepared nitrate solutions were mixed in the desired stoichiometric ratios in a quartz beaker with glycine (>98.5% pure, Acros), at a ratio of 0.56 mol glycine/mol nitrate. The mixture was heated until a gel was formed and then combusted, producing a dry powder. These powders were subsequently calcined in air at 700 °C for 1 h. For testing in the ATR reactor, the powders were dry-pressed into pellets, lightly crushed, and then sieved to a particle size of −20/+40 mesh.

2.2. Catalytic Testing. A small-scale, fixed-bed, plug-flow reactor was used for the catalytic ATR experiments. The sieved samples were loaded into the reactor catalyst bed, which was heated externally using a resistance furnace (Lindberg). The catalyst sample holder consisted of a $^1/_2$-in. outer diameter (O.D.) stainless steel tube with $^1/_{16}$-in.-thick aluminosilicate felt pads at the top and bottom. Thermocouples that touched the felt pads at the inlet side and outlet side of the catalyst bed were used to monitor the internal reactor temperatures, while a thermocouple external to the reactor tube was used to control the furnace temperature. The reactor also had pressure gauges installed at the inlet and outlet of the catalyst bed to monitor the pressure buildup that might occur due to coking. Separate HPLC pumps (Alltech) were used to deliver the water and liquid fuel to the vaporizer, which was heated to 200 °C and used a nitrogen sweep gas. Separate mass-flow controllers delivered the required amounts of oxygen and nitrogen to the reactor at a point downstream of the vaporizer and upstream of the catalyst bed inlet. An online gas chromatograph (Hewlett-Packard, Model 6890) with a flame ion detector and a thermal conductivity detector were used to determine the composition of the reaction products flowing out from the catalyst bed. At the end of the ATR tests, the fuel, water, oxygen, and nitrogen flows were all shut down simultaneously, immediately followed by cooling of the furnace to avoid any oxidizing or coking conditions.

An initial "light-off" test was conducted with 1.2 mL (1.5 g) of the $La_{0.8}Sr_{0.2}Cr_{0.9}Ni_{0.1}O_{3\pm\delta}$ catalyst. The fuel was isooctane (2,2,4-trimethylpentane, C_8H_{18}), the oxygen-to-carbon (O_2:C) ratio was 0.49, the steam-to-carbon (H_2O:C) ratio was 1.3, and the space velocity was 17 000 h^{-1}. The space velocity is calculated by dividing the volume of catalyst by the volumetric flow rate of the reactants, which is calculated from the molar flow rate using the ideal gas law in the case of the liquids. First, the temperature of the furnace was ramped up from 550 °C to 750 °C in 50 °C increments with 45-min holds at each temperature. Three gas chromatography (GC) samples of the products were taken at each temperature at 15-min intervals. Next, the temperature of the furnace was ramped down in 50 °C intervals.

To obtain the used catalyst samples for neutron diffraction studies, 4 mL (4−5 g) of the sieved perovskite samples were subjected to the ATR reaction over a period of 6.5 h using isooctane as the hydrocarbon fuel. The O_2:C ratio was maintained at 0.49, the H_2O:C ratio was maintained at 1.2, and the space velocity was maintained at 16 000 h^{-1}. The furnace temperature was set at 700 °C, resulting in catalyst temperatures that ranged from 740 °C to 770 °C on the inlet side to 680−690 °C on the outlet side, except in the case of $LaMn_{0.9}Ni_{0.1}O_{3\pm\delta}$, where the inlet temperature rose to 860 °C for 1 h near the beginning of the test.

2.2.1. Safety Precautions for Catalytic Tests. The reactor described above was set up inside a large fume hood with an internal volume of 3567 L, an exhaust flow velocity of 3681 L/min, and a hood flow alarm. No other experiments or equipment were co-located inside this hood. All experiments were conducted during normal daytime working hours, and no experiments were performed unattended. After each catalyst was loaded into the reactor, the system was checked for leaks by pressurizing it with N_2, and then stopping the N_2 flow; a pressure gauge at the inlet of the reactor would show a pressure drop if there was a leak in the system. The experiments were conducted under constant flow, and the system was not closed during testing. If the pressure inside the reactor started to increase because of severe coking of the catalyst, there was a pressure relief valve upstream

(19) Peña, M. A.; Fierro, J. L. G. *Chem. Rev.* **2001**, *101*, 1981–2017.
(20) Dong, W.; Jun, K.; Roh, H.; Liu, Z.; Park, S. *Catal. Lett.* **2002**, *78*, 215–222.
(21) Pino, L.; Recupero, V.; Beninati, S.; Shukla, A. K.; Hegde, M. S.; Bera, P. *Appl. Catal., A* **2002**, *225*, 63–75.
(22) Rauch, H.; Waschkowski, W. *Neutron Scattering Lengths*; Springer−Verlag: Berlin, 2000; Vol. *16A1*, Chapter 6.
(23) Chick, L. A.; Pederson, L. R.; Maupin, G. D.; Bates, J. L.; Thomas, L. E.; Exarhos, G. J. *Mater. Lett.* **1990**, *10*, 6–12.

of the catalyst bed that would open and vent the gases into the hood exhaust. Most of the effluent from the reactor was also fed directly to the hood exhaust. Only small portions of the effluent flowed to the GC apparatus, which would show any downstream leaks as an O_2 peak, because all O_2 fed into the reactor was consumed in the reaction. Under the conditions that we used for our experiments in this study, the most H_2 produced was 450 mL/min. At this rate, it would take more than 5 h to reach the 4% flammability limit inside the hood if the exhaust fans shut down. But, any significant drop in exhaust flow would trigger the hood flow alarm and signal the experimenter to turn off the reactor.

2.3. Catalyst Characterization. Before catalytic testing, conventional powder XRD (Hitachi) was used to verify that the as-prepared catalyst powders were single-phase with the perovskite structure. All used catalyst samples were also analyzed by powder XRD. The Brunauer−Emmett−Teller (BET) surface area of the catalysts before and after testing was measured using nitrogen adsorption at 77 K (Micromeritics, Model ASAP 2010). Samples were analyzed for carbon deposition after testing using a combustion analysis method (LECO). Eight catalyst samples were taken to the Intense Pulsed Neutron Source (IPNS) at Argonne National Laboratory for a more-sensitive determination of the phases present. The neutron diffraction data were collected *ex situ* under atmospheric conditions at room temperature. Neutron difraction data in the range of 0.8−4.0 Å were analyzed using the GSAS Rietveld software package.[24] Refinements were performed in a manner as previously reported,[25−27] yielding crystallographic data including phases present, crystallographic space group, and lattice parameters. All samples were also examined using a field-emission scanning electron microscopy (FE-SEM) microscope (Hitachi, Model S-4700-II) and the three tested, strontium-doped samples were examined in a conventional transmission electron microscopy (TEM) microscope (Philips, Model CM-30T) that was equipped with an energy-dispersive X-ray (EDAX) spectrometer. The TEM samples were prepared by dispersing a small amount of each catalyst in ethanol and then placing a drop of the dispersion onto a gold grid that was covered by a thin carbon film. The TEM system was operated at an accelerating voltage of 200 kV.

3. Results

3.1. Catalytic Autothermal Reforming. The catalytic testing results are reported in terms of "product yield", which is defined as the molar flow rate of a given gas species out of the reactor divided by the molar flow rate of the C_8H_{18} vapor into the reactor. The results from the initial test are shown in Figure 1. This test shows that light-off (when 50% of the C_8H_{18} is converted to hydrogen) happens when the catalyst is at a temperature of ~675 °C. It can also be seen that CO yields increase at temperatures above 625 °C, because of incomplete oxidation of the hydrocarbon. For these tests, 100% conversion of the isooctane feed was observed only at 750 °C

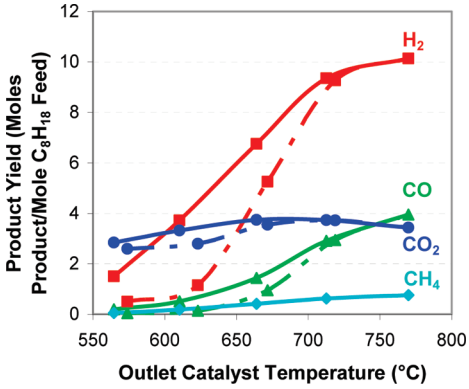

Figure 1. Results of the catalyst light-off test for $La_{0.8}Sr_{0.2}Cr_{0.9}Ni_{0.1}O_{3\pm\delta}$. The dashed lines represent data taken as the furnace temperature was increased, and the solid lines represent data taken as the furnace temperature was reduced. The errors in the yields are ±0.1 mol product/mol C_8H_{18} for H_2, ±0.08 mol product/mol C_8H_{18} for CO, and ±0.02 mol product/mol C_8H_{18} for CO_2 and CH_4.

with only a small amount of non-methane hydrocarbon breakthrough, ~0.004 mol C_2/mol C_8H_{18}, and 0.004 mol of C_3/mol C_8H_{18} feed. At lower temperatures, the presence of CO_2 in the product stream without much CO or H_2 indicated that oxidation of part of the fuel was occurring, but not steam reforming. As is typical of nickel-containing perovskites, there was some hysteresis in the hydrogen and CO yields, with the decreasing-temperature yields being higher than the increasing-temperature yields. This is believed to be due to metallic nickel, which is known to promote steam reforming, being produced on the surface of the perovskite due to the reducing conditions resulting from ATR. Because the conditions are the most reducing at the highest temperature, an enhancement effect from the metallic nickel is observed when the temperature is decreased. Powder XRD (see the diffraction patterns shown in Figure 2) was not sensitive enough to confirm the presence of small amounts of metallic nickel in either the sample used for the light-off test or the samples tested for 6.5 h at 700 °C.

Figure 3 shows the product yield versus time of the $LaCr_{0.9}Ni_{0.1}O_{3\pm\delta}$ catalyst that was later characterized by neutron diffraction. This catalyst had the best performance of the six compositions tested. Not shown in Figure 3 is the small amount of isooctane breakthrough, which was no more than 0.02 mol/mol feed input. Figure 3 shows that the performance of the catalyst degraded slightly over the 6.5 h test period. This is typical of these catalysts, and it is likely due either to a small amount of carbon deposition on the surface of the catalyst, which would block active sites, or to sintering of the catalyst, resulting in a loss of surface area and a reduction in the number of active surface sites. A summary of the hydrogen production results of the 6.5 h tests, along with the results of BET surface area measurements, and the carbon content measurements of the six catalyst compositions is given in Table 1.

The effect on catalytic performance of doping with strontium on the A-site of the perovskite, i.e., $La_{1-x}Sr_xM_{1-x}Ni_xO_{3\pm\delta}$ (where M = Cr, Mn, or Fe and $x = 0.1$), is shown in Figure 4. This figure shows that the

(24) Larson, A. C.; Von Dreele, R. B. *General Structure Analysis System (GSAS)*; Los Alamos National Laboratory: Los Alamos, CA, 2000.
(25) Kim, J. S.; Vaughey, J. T.; Johnson, C. S.; Thackeray, M. M. *J. Electrochem. Soc.* **2003**, *150*, A1498–A1502.
(26) Vaughey, J. T.; Harrison, W. T. A.; Jacobson, A. J.; Goshorn, D. P.; Johnson, J. W. *Inorg. Chem.* **1994**, *33*, 2481–2487.
(27) Vaughey, J. T.; Hasty, E. F.; Poeppelmeier, K. R. *Solid State Ionics* **1992**, *53−56*, 573–577.

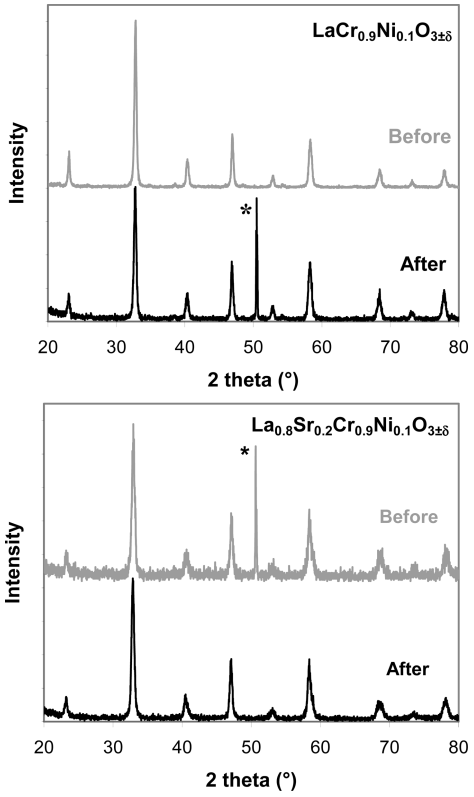

Figure 2. Powder X-ray diffraction (XRD) patterns of two catalysts before and after ATR tests: (a) $LaCr_{0.9}Ni_{0.1}O_{3\pm\delta}$ and (b) $La_{0.8}Sr_{0.2}Cr_{0.9}Ni_{0.1}O_{3\pm\delta}$ catalyst. The peaks marked with an asterisk (*) are sample holder peaks. All other peaks correspond to $LaCrO_3$.[39]

doping with strontium on the A-site had little effect on the hydrogen production for the chromium-containing composition; it significantly improved hydrogen production for the manganese-containing composition; and it decreased hydrogen production for the iron-containing composition. Although the strontium doping had little effect on the H_2 yield of the chromates, when the isooctane breakthrough and CO yields of $La_{0.8}Sr_{0.2}Cr_{0.9}Ni_{0.1}O_{3\pm\delta}$ and $LaCr_{0.9}Ni_{0.1}O_{3\pm\delta}$ are compared, $LaCr_{0.9}Ni_{0.1}O_{3\pm\delta}$ performed slightly better than $La_{0.8}Sr_{0.2}Cr_{0.9}Ni_{0.1}O_{3\pm\delta}$, producing more CO and allowing less C_8H_{18} breakthrough, as seen in Table 1. These tests showed that (i) using chromium as the stabilizing element on the B-site gives the best performance, and (ii) the effect of doping with strontium on the A-site varies, depending on the cation on the B-site.

Table 1 also shows the results of the carbon content analysis. Note that the $La_{0.8}Sr_{0.2}Cr_{0.9}Ni_{0.1}O_{3\pm\delta}$ powder had a carbon content of 0.98 wt % before testing and the $La_{0.8}Sr_{0.2}Mn_{0.9}Ni_{0.1}O_{3\pm\delta}$ had a carbon content of 0.57 wt % before testing, whereas all the others had a carbon content of 0.18 wt % or lower before testing. For the chromium-containing catalysts, no carbon deposition was observed. In the case of $La_{0.8}Sr_{0.2}Cr_{0.9}Ni_{0.1}O_{3\pm\delta}$, for which there was a high carbon content before testing, the carbon content actually decreased significantly. In the case of $La_{0.8}Sr_{0.2}Mn_{0.9}Ni_{0.1}O_{3\pm\delta}$, which also had a high carbon content before testing, there was only a small amount of additional carbon in the tested material, which

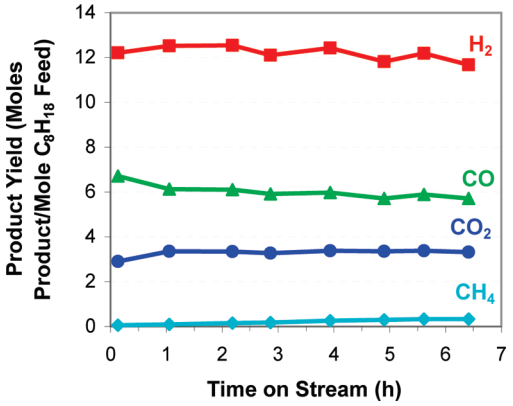

Figure 3. Product yield versus time for autothermal reforming (ATR) of C_8H_{18} with the $LaCr_{0.9}Ni_{0.1}O_{3\pm\delta}$ catalyst. The errors in the yields are ±0.1 mol product/mol C_8H_{18} for H_2, ±0.04 mol product/mol C_8H_{18} for CO, and ±0.02 mol product/mol C_8H_{18} for CO_2 and CH_4.

can be attributed to the presence of a carbonate phase (see section 3.2). However, the undoped analog, $LaMn_{0.9}Ni_{0.1}O_{3\pm\delta}$ had the most carbon deposition after testing—1.7 wt %. The carbon deposition on this catalyst may be the result of pyrolysis reactions that occurred due to the higher inlet temperature that was observed during the testing of this sample. The iron-containing catalysts did show small amounts of carbon deposition, which was more pronounced for the strontium-doped composition.

3.2. Neutron Diffraction. The eight samples examined using neutron powder diffraction are listed in Table 2. The atomic positions, thermal factors, occupancy, lattice parameters, and phase distribution and identification were determined by the Rietveld refinement of the neutron diffraction data, using the program GSAS.[24] A more in-depth description of the refinements was recently reported in a separate publication.[28] All six of the catalytically tested samples had metallic nickel present in them. The extremely high sensitivity of neutron diffraction methods to the presence of nickel makes it a good tool for identifying even minute quantities of it in a sample. In five of those six samples, the only other phase detected was a perovskite, indicating it should be B-site-deficient, because of the loss of nickel from the perovskite structure. Similar synthetic techniques have also been reported to form B-site-deficient perovskites for the perovskites $SrRu_{1-v}O_{3\pm\delta}$[29] and $LaMn_{1-x}O_{3\pm\delta}$.[30] In the tested $La_{0.8}Sr_{0.2}Mn_{0.9}Ni_{0.1}O_{3\pm\delta}$ and $LaMn_{0.9}Ni_{0.1}O_{3\pm\delta}$ samples, the perovskite phase that remained had orthorhombic symmetry. In the other six samples, the nickel doping introduces a monoclinic distortion into the ideally cubic perovskite structure. This reduction in symmetry to monoclinic creates two separate B-cation sites that allow the cations to sit on two sites with slightly different oxygen bond lengths.[28]

(28) Vaughey, J. T.; Mawdsley, J. R.; Krause, T. R. *Mater. Res. Bull.* **2007**, *42*, 1963–1968.
(29) Dabrowski, B.; Chmaissem, O.; Klamut, P. W.; Kolesnik, S.; Maxwell, M.; Mais, J.; Ito, Y.; Armstrong, B. D.; Jorgensen, J. D.; Short, S. Phys. Rev. B **2004**, *70*.
(30) Topfer, J.; Goodenough, J. B. *J. Solid State Chem.* **1997**, *130*, 117–128.

Table 1. Results from the Autothermal Reforming Experiments, Carbon Content Analysis, and BET Surface Area Measurements

	BET Surface Area of Catalyst (m^2/g)[a]		6.5 h Performance Results		Carbon Content of Catalyst (wt %)[b]	
composition	as-prepared	tested	H_2 yield (mol/mol C_8H_{18} feed)[c]	C_8H_{18} break-through (%)[d]	as-prepared	tested
$La_{0.8}Sr_{0.2}Cr_{0.9}Ni_{0.1}O_{3\pm\delta}$	12.1	12.7	11.9	5.2	0.98	0.22
$LaCr_{0.9}Ni_{0.1}O_{3\pm\delta}$	13.1	10.6	11.7	1.7	0.10	0.10 ± 0.02
$La_{0.8}Sr_{0.2}Mn_{0.9}Ni_{0.1}O_{3\pm\delta}$	16.7	3.2	11.4	3.7	0.57	0.67
$LaMn_{0.9}Ni_{0.1}O_{3\pm\delta}$	26.5	7.6	9.8	3.9	0.18 ± 0.02	1.74 ± 0.10
$La_{0.8}Sr_{0.2}Fe_{0.9}Ni_{0.1}O_{3\pm\delta}$	2.7	2.9	10.5	8.5	0.034	0.21
$LaFe_{0.9}Ni_{0.1}O_{3\pm\delta}$	2.6	2.4	11.3	7.5	0.035	0.08 ± 0.02

[a] The error in the BET measurements is 0.1 m^2/g. [b] The error in the carbon content is ±5% of the reported value, unless otherwise noted. [c] The error in the H_2 yield is 0.1 mol/mol C_8H_{18}. [d] The error in the C_8H_{18} breakthrough is 0.9%.

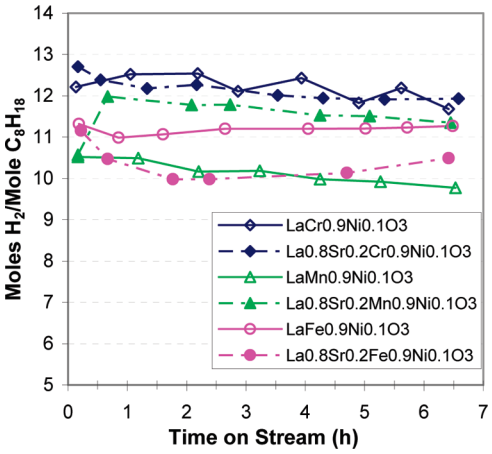

Figure 4. Comparison of the hydrogen yield of six perovskite catalysts, showing the varying effects of strontium doping on the A-site. The error in the hydrogen yield was 0.1 mol H_2/mol C_8H_{18}.

Undoped $LaCrO_3$ is an orthorhombic perovskite (space group *Pbnm*) with only one distinct metal site.[31] Our as-prepared $La_{0.8}Sr_{0.2}Cr_{0.9}Ni_{0.1}O_{3\pm\delta}$ catalyst was determined to be a single-phase perovskite material with a slight monoclinic distortion. The lattice constants were determined to be a = 5.4759(7) Å, b = 5.4996(6) Å, c = 7.7572(12) Å, and β = 90.692(8)° in the space group $P2_1/n$. The oxygen positions were determined to be fully occupied upon refinement, but the nickel seems to segregate to the smaller of the two octahedral positions. Because nickel segregates to this one site, all of the (Ni/Cr)/O octahedra are surrounded by pure Cr/O octahedra. As a consequence, any oxygen loss by the nickel-based octahedra causes a surrounding Cr(III)/O octahedra to lose oxygen and reduce its coordination to square pyramidal or tetrahedral. This is thermodynamically unfavorable;[32] therefore, the ability of the perovskite to lose oxygen is limited. The tested $La_{0.8}Sr_{0.2}Cr_{0.9}Ni_{0.1}O_{3\pm\delta}$ catalyst was refined best as a perovskite with monoclinic distortion and 0.4% metallic nickel. The lattice constants of the perovskite phase were determined to be a = 5.4805(6) Å, b = 5.5022(5) Å, c = 7.7637(11) Å, and β = 90.645(8)° in space group $P2_1/n$. Figure 5a shows the region of the neutron diffraction patterns of the as-prepared and tested $La_{0.8}Sr_{0.2}Cr_{0.9}Ni_{0.1}O_{3\pm\delta}$ between 1.5 and 3 Å. The finding of nickel separation from the perovskite is consistent with the findings of Sfeir et al., who, using transmission electron microscopy, observed nickel islets on $La_{0.85}Ca_{0.15}Cr_{0.9}Ni_{0.1}O_{3\pm\delta}$ after methane partial oxidation and steam reforming tests.[12] The tested $LaCr_{0.9}Ni_{0.1}O_{3\pm\delta}$ catalyst gave similar results, exhibiting a B-site-deficient perovskite with monoclinic distortion and 0.31% metallic nickel.

$La_{0.8}Sr_{0.2}MnO_{3\pm\delta}$ is a monoclinic perovskite belonging to the space group $P2_1/c$.[33] The neutron diffraction pattern of our as-prepared $La_{0.8}Sr_{0.2}Mn_{0.9}Ni_{0.1}O_{3\pm\delta}$ was refined to a single phase, monoclinically distorted perovskite. The lattice constants are a = 5.4913(8) Å, b = 5.5036(7) Å, c = 7.7867(17) Å, and β = 90.626(10)° in space group $P2_1/n$. As with the chromium-based samples, the refinement showed that the Ni atoms were all on the smaller of the two octahedral positions. The tested $La_{0.8}Sr_{0.2}Mn_{0.9}Ni_{0.1}O_{3\pm\delta}$ was determined to have decomposed under our test conditions and was determined to be a mixture of 87.5% (La, Sr)$MnO_{3\pm\delta}$ perovskite, 1.6% nickel metal, 3.8% $La_2O_2CO_3$, 4.3% $SrCO_3$, and 2.8% Mn_2O_3. The lattice constants of the remaining perovskite phase were a = 5.541(8) Å, b = 5.6538(7) Å, and c = 7.7669(12) Å in space group *Pbnm*. These matched well with those reported for (La,Sr)$MnO_{3\pm\delta}$.[34] Figure 5b shows the neutron diffraction patterns of the as-prepared and tested $La_{0.8}Sr_{0.2}Mn_{0.9}Ni_{0.1}O_{3\pm\delta}$. In addition, the tested strontium-free analog, $LaMn_{0.9}Ni_{0.1}O_{3\pm\delta}$, was evaluated. Similar to the previous phases, it was determined to lose a small amount of nickel from the perovskite lattice but with retention of the perovskite structure from the residual material.

$La_{0.8}Sr_{0.2}FeO_{3\pm\delta}$ is an orthorhombic perovskite belonging to the space group *Pbnm*.[35] Our tested $La_{0.8}Sr_{0.2}Fe_{0.9}Ni_{0.1}O_{3\pm\delta}$ was refined best as a mixture of a distorted B-cation-deficient perovskite with a monoclinic distortion and 2.08% free nickel metal. As shown in Table 2, refinement gives the lattice constants of the residual perovskite to be a = 5.5418(3) Å, b = 5.5488(4) Å, c = 7.8361(8) Å, and β = 90.246(4)° in space group $P2_1/n$. Because of the loss of 7.7 wt % nickel, the residual perovskite has a larger B-site deficiency than other

(31) JCPDS−ICDD File Card No. 33-0701; International Centre for Diffraction Data: Newtowne Square, PA
(32) Nakamura, T.; Petzow, G.; Gauckler, L. J. *Mater. Res. Bull.* **1979**, *14*, 649–659.
(33) JCPDS−ICDD File Card No. 40-1100; International Centre for Diffraction Data: Newtowne Square, PA
(34) Dabrowski, B.; Xiong, X.; Bukowski, Z.; Dybzinski, R.; Klamut, P. W.; Siewenie, J. E.; Chmaissem, O.; Shaffer, J.; Kimball, C. W.; Jorgensen, J. D.; Short, S. *Phys. Rev. B* **1999**, *60*, 7006–7017.
(35) Dann, S. E.; Currie, D. B.; Weller, M. T.; Thomas, M. F.; Alrawwas, A. D. *J. Solid State Chem.* **1994**, *109*, 134–144.

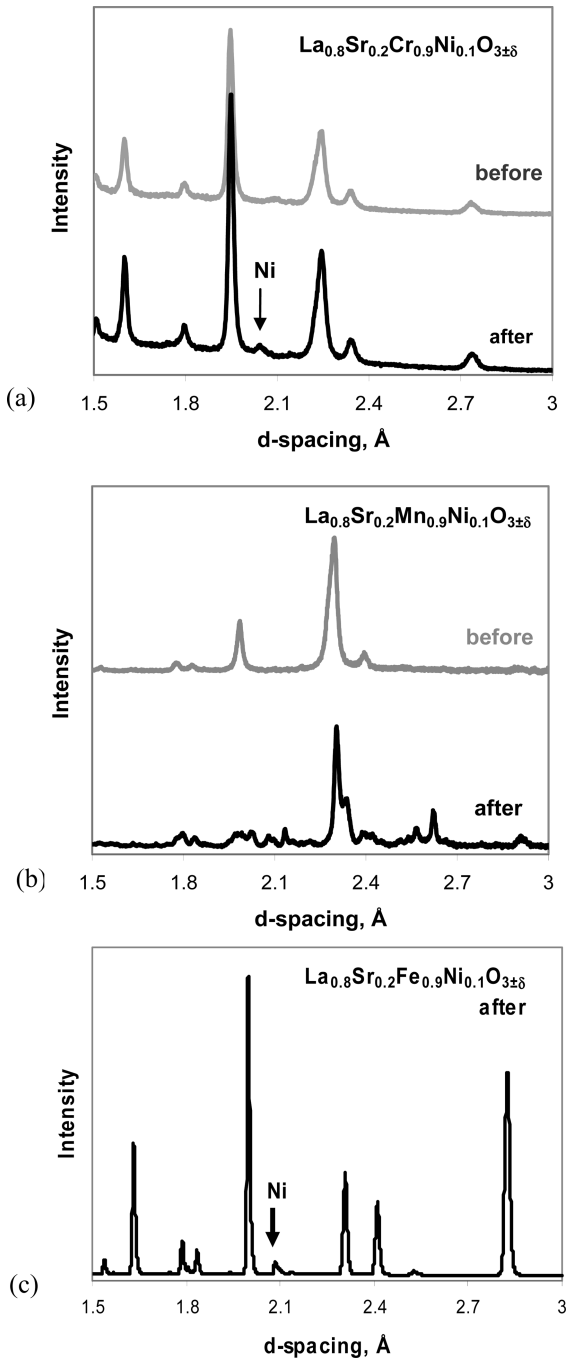

Figure 5. Neutron diffraction patterns of the (a) $La_{0.8}Sr_{0.2}Cr_{0.9}Ni_{0.1}O_{3\pm\delta}$ catalyst before and after testing with 2,2,4-trimethylpentane fuel for 6.5 h, (b) $La_{0.8}Sr_{0.2}Mn_{0.9}Ni_{0.1}O_{3\pm\delta}$ catalyst before and after testing with 2,2,4-trimethylpentane fuel for 6.5 h, and (c) $La_{0.8}Sr_{0.2}Fe_{0.9}Ni_{0.1}O_{3\pm\delta}$ catalyst after testing with 2,2,4-trimethylpentane fuel for 6.5 h.

samples evaluated. The larger loss may highlight the influence of Cr(III) in the other samples and its ability to hold oxygen in the lattice, limiting the loss of nickel to sites near the surface of the crystallites.[36] One would expect that a loss of nickel this great would result in the original perovskite falling apart, as in the case of $La_{0.8}Sr_{0.2}Mn_{0.9}Ni_{0.1}O_{3\pm\delta}$. In the refinement, the isotropic temperature factors (Bisos) for the oxygen positions were determined to have large errors, indicating an uncertainty in their exact position or occupancy.

Figure 5c shows the neutron diffraction pattern of the tested $La_{0.8}Sr_{0.2}Fe_{0.9}Ni_{0.1}O_{3\pm\delta}$. Both this sample and the tested strontium-free analog, were determined to be a mixture of metallic nickel and a B-site-deficient perovskite. As compared to $La_{0.8}Sr_{0.2}Fe_{0.9}Ni_{0.1}O_{3\pm\delta}$, $LaFe_{0.9}Ni_{0.1}O_{3\pm\delta}$ only lost half the amount of nickel, which may reflect the added structural instabilities created by strontium doping.

The neutron diffraction measurements, shown in Table 2, did not reveal any graphitic or crystalline carbon in any of the samples; carbon was observed as carbonate, but only definitively identified in the tested $La_{0.8}Sr_{0.2}Mn_{0.9}Ni_{0.1}O_{3\pm\delta}$ sample. So, in the samples where carbon deposition was detected using LECO analysis (i.e., $LaMn_{0.9}Ni_{0.1}O_{3\pm\delta}$, $La_{0.8}Sr_{0.2}Fe_{0.9}Ni_{0.1}O_{3\pm\delta}$, and $LaFe_{0.9}Ni_{0.1}O_{3\pm\delta}$, as shown in Table 1), the carbon must have been present in amorphous form. Although crystalline forms of carbon, such as nanotubes, have been shown to form on perovskite catalysts during ATR,[9] and they are often associated with the presence of metallic nickel particles,[37] the reforming conditions used in this study—aromatic-free and sulfur-free fuel plus a relatively short time-on-stream—must have favored the formation of amorphous carbon.

3.3. Electron Microscopy. All eight samples that were analyzed via neutron diffraction were also examined via SEM, as shown by the micrographs in Figure 6a−c for the tested strontium-doped catalysts. It can be seen that the relative particle sizes of the oxide phases of the three compositions correlate well with the BET surface area measurements shown in Table 1. On the $La_{0.8}Sr_{0.2}Fe_{0.9}Ni_{0.1}O_{3\pm\delta}$ (Figure 6a) samples and the $La_{0.8}Sr_{0.2}Mn_{0.9}Ni_{0.1}O_{3\pm\delta}$ (Figure 6b) samples, it can be seen that there are smaller particles on bigger particles. The spherical morphology of the smaller particles is consistent with a metal particle on an oxide substrate, because it is well-known that metals do not wet oxide surfaces. The neutron diffraction data indicate that, in the iron-containing sample, these smaller particles are likely nickel and the larger particles are the remaining, B-site-deficient perovskite phase. The SEM micrographs of tested $LaFe_{0.9}Ni_{0.1}O_{3\pm\delta}$ catalyst look similar to those of its strontium-doped analog, $La_{0.8}Sr_{0.2}Fe_{0.9}Ni_{0.1}O_{3\pm\delta}$, with the difference being that the nickel particles are smaller. These smaller spherical particles were not observed on the as-prepared versions of these three samples. A second phase that might also be nickel particles could not be resolved for the $La_{0.8}Sr_{0.2}Cr_{0.9}Ni_{0.1}O_{3\pm\delta}$ (Figure 6c) and $LaCr_{0.9}Ni_{0.1}O_{3\pm\delta}$ samples by SEM, which suggests that the nickel particles are <9 nm in size. The SEM micrographs of the tested $LaMn_{0.9}Ni_{0.1}O_{3\pm\delta}$ sample revealed what seemed to be many amorphous carbon filaments ~50−100 nm in diameter, which is consistent with the higher carbon content measured by LECO for this sample. For this sample, the nickel particles may have been inside or on top of the carbon filaments.

(36) Thursfield, A.; Metcalfe, I. S.; Kruth, A.; Irvine, J. T. S. In *Metal Oxides: Chemistry and Applications*; Fierro, J. L. G., Ed.; CRC Press: Boca Raton, FL, 2006; pp 55−85.

(37) Trimm, D. L. *Catal. Today* **1999**, *49*, 3–10.

Table 2. Lattice Parameters and Phase Content from Neutron Diffraction Data Analysis

composition	space group	Lattice Constants				phase fraction
		a (Å)	*b* (Å)	*c* (Å)	*β* (°)	
$La_{0.8}Sr_{0.2}Cr_{0.9}Ni_{0.1}O_{3\pm\delta}$ (as-prepared)	$P2_1/n$	5.4759(7)	5.4996(6)	7.7572(12)	90.692(8)	100% perovskite
$La_{0.8}Sr_{0.2}Cr_{0.9}Ni_{0.1}O_{3\pm\delta}$ (tested)	$P2_1/n$	5.4805(6)	5.5022(5)	7.7637(11)	90.645(8)	0.43% Ni, 99.57% perovskite
$LaCr_{0.9}Ni_{0.1}O_{3\pm\delta}$ (tested)	$P2_1/n$	5.4909(5)	5.4941(4)	7.7672(6)	90.386(6)	0.31% Ni, 99.69% perovskite
$La_{0.8}Sr_{0.2}Mn_{0.9}Ni_{0.1}O_{3\pm\delta}$ (as-prepared)	$P2_1/n$	5.4913(8)	5.5036(7)	7.7867(17)	90.626(10)	100% perovskite
$La_{0.8}Sr_{0.2}Mn_{0.9}Ni_{0.1}O_{3\pm\delta}$ (tested)	*Pbnm*	5.541(8)	5.6538(7)	7.7669(12)	n/a	1.6% Ni, 87.5% perovskite, 4.3% $SrCO_3$, 3.8% $La_2O_2CO_3$, 2.8% Mn_2O_3
$LaMn_{0.9}Ni_{0.1}O_{3\pm\delta}$ (tested)	*Pbnm*	5.5232(4)	5.6168(5)	7.7452(8)	n/a	1.2% nickel, 98.8% perovskite
$La_{0.8}Sr_{0.2}Fe_{0.9}Ni_{0.1}O_{3\pm\delta}$ (tested)	$P2_1/n$	5.5418(3)	5.5488(4)	7.8361(8)	90.246(4)	2.08% nickel, 97.92% perovskite
$LaFe_{0.9}Ni_{0.1}O_{3\pm\delta}$ (tested)	$P2_1/n$	5.5551(2)	5.5613(2)	7.8487(2)	90.078(3)	1.02% nickel, 98.98% perovskite

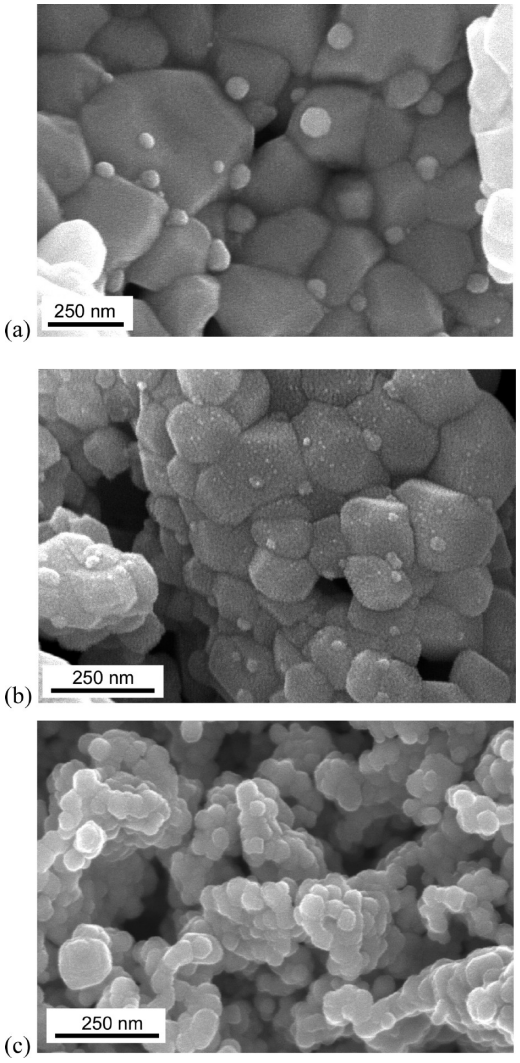

Figure 6. SEM micrographs of the tested strontium-doped perovskite catalysts: (a) $La_{0.8}Sr_{0.2}Fe_{0.9}Ni_{0.1}O_{3\pm\delta}$, (b) $La_{0.8}Sr_{0.2}Mn_{0.9}Ni_{0.1}O_{3\pm\delta}$, and (c) $La_{0.8}Sr_{0.2}Cr_{0.9}Ni_{0.1}O_{3\pm\delta}$.

In the TEM analysis, nickel particles were identified on the surfaces of the $La_{0.8}Sr_{0.2}Fe_{0.9}Ni_{0.1}O_{3\pm\delta}$ and $La_{0.8}Sr_{0.2}Mn_{0.9}Ni_{0.1}O_{3\pm\delta}$ catalysts using energy dispersive X-ray spectrometry. Two representative bright-field images from these samples are shown in Figures 7a and 7b. These results confirm that the smaller particles observed in the SEM images are the free nickel that was detected by neutron diffraction. Also, areas that were high in manganese or strontium were found in the $La_{0.8}Sr_{0.2}Mn_{0.9}Ni_{0.1}O_{3\pm\delta}$ sample, as would be expected from the neutron diffraction data.

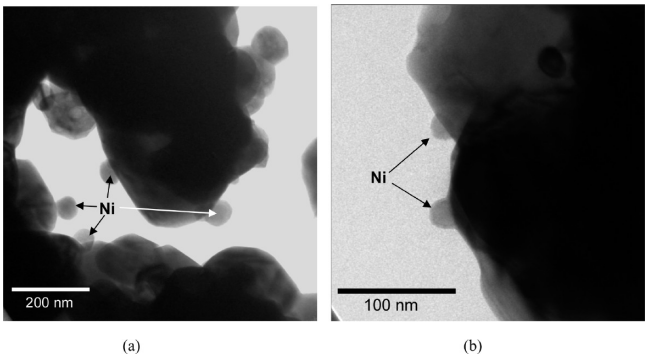

Figure 7. TEM bright-field images of (a) $La_{0.8}Sr_{0.2}Fe_{0.9}Ni_{0.1}O_{3\pm\delta}$ and (b) $La_{0.8}Sr_{0.2}Mn_{0.9}Ni_{0.1}O_{3\pm\delta}$ after testing with 2,2,4-trimethylpentane fuel for 6.5 h. The smaller particles on the surfaces of the larger particles were determined to be nickel, using EDX.

Nickel particles could not be found on the $La_{0.8}Sr_{0.2}Cr_{0.9}Ni_{0.1}O_{3\pm\delta}$ catalyst. This may be because the Ni particles were such a small fraction of the sample and also because there were many perovskite particles under 50 nm, so the metallic particles would not stand out so much due to size difference, as was the case for the other two samples.

4. Discussion

Nickel oxide is known to be less thermodynamically stable in a reducing atmosphere than the parent perovskite phases, $LaMO_3$ (where, in this study, M = Cr, Mn, Fe).[32] Nakamura et al.[32] conducted a thermogravimetric study on NiO and various $LaMO_3$ perovskites, including $LaCrO_3$, $LaMnO_3$, $LaFeO_3$, and $LaNiO_3$ at 1000 °C in reducing atmospheres. In their study, $LaCrO_3$ was not reduced, even at the lowest p_{O_2} tested (7.9×10^{-22} bar), $LaMnO_3$ was destabilized to La_2O_3 and MnO at $p_{O_2} = 8.9 \times 10^{-16}$ bar, $LaFeO_3$ was reduced to La_2O_3 and Fe at $p_{O_2} = 1.1 \times 10^{-17}$ bar, and NiO was reduced to nickel at $p_{O_2} = 2.8 \times 10^{-11}$ bar. They found that $LaNiO_3$ forms La_2NiO_4 + NiO at $p_{O_2} = 0.25$ bar, which then forms metallic Ni at $p_{O_2} = 6.8 \times 10^{-12}$ bar, so the incorporation of nickel into a binary oxide does impart a small amount of reduction resistance. This has also been observed for the perovskite compound $LaGa_{0.65}Mg_{0.15}Ni_{0.2}O_{3-\delta}$.[38] At lower temperatures, such as in our experiments, reduction

(38) Yaremchenko, A. A.; Kharton, V. V.; Naumovich, E. N.; Shestakov, D. I.; Chukharev, V. F.; Kovalevsky, A. V.; Shaula, A. L.; Patrakeev, M. V.; Frade, J. R.; Marques, F. M. B. *Solid State Ionics* **2006**, *177*, 549–558.
(39) JCPDS–ICDD File Card No. 24-1016; International Centre for Diffraction Data: Newtowne Square, PA

is less thermodynamically favored, so that a lower p_{O_2} is required to achieve the same extent of reduction. Thermodynamic calculations using HSC Chemistry software (version 5.0) indicate that, at 700 °C, NiO reduces to nickel at $p_{O_2} = 6.3 \times 10^{-17}$ bar. We did not measure the p_{O_2} in our reactor; however, using HSC Chemistry software, we estimate that, at 700 °C, it was 1.6×10^{-23} bar, which is low enough to reduce NiO to metallic nickel, even with a small amount of increased reduction resistance, because of incorporation into a perovskite structure.

Conventional powder XRD, shown in Figure 2, was not sensitive enough to confirm the presence of small amounts of metallic nickel in either the sample used for the light-off tests or the samples tested for 6.5 h at 700 °C. Therefore, neutron diffraction was chosen as the technique to confirm and quantify the presence of metallic nickel in the used catalysts, as shown in Figures 5a−c. Neutron diffraction is useful for these types of materials, because oxygen and nickel have very large scattering cross sections for neutrons,[22] in contrast to XRD, where scattering strength scales to atomic number, so small changes in the oxygen anion position or thermal factor would be difficult to detect. In addition, the metallic nickel particles that are formed on the surface would be hard to detect against the background of the samples using XRD, because of a combination of small particle size and relative amount. We had speculated in an earlier study, based on an examination of our product distribution,[9] that metallic nickel particles had formed on perovskite catalysts of the same compositions as those used in this study. In the previous study, however, the fuels used contained aromatics and sulfur, both of which promote coke formation, and the time-on-stream was longer than in the present study; thus, the ATR conditions used this study would not be considered especially harsh, in comparison. Yet, the results of the neutron diffraction experiments performed in this study confirm that metallic nickel particles had formed in the perovskite catalysts, but at levels too low to be detected by conventional powder XRD.

Ex situ neutron diffraction revealed that the different compositions adjusted to the reducing environment of the autothermal reforming reactor via different mechanisms. The two chromium-containing samples lost the least amount of nickel from the perovskite structure, roughly 0.3−0.4%, as compared to the other samples, which had 1−2% metallic nickel, as seen in Table 2. This is probably due to the fact that, thermodynamically, chromates are more stable and reduction resistant than the manganate and ferrate analogs.[32] Table 2 also shows that the strontium-containing samples lost more nickel from their perovskite lattices than the strontium-free analogs. This is likely the result of the strontium doping creating oxygen vacancies in the perovskite crystal lattice, which can then promote the reduction reaction that frees the Ni, as has been observed by Yaremchenko et al.[38] This phenomenon also explains why the $La_{0.8}Sr_{0.2}Mn_{0.9}Ni_{0.1}O_{3\pm\delta}$ sample exhibited a breakdown of some of the perovskite structure that accompanied the loss of nickel from the parent perovskite phase, while the $LaMn_{0.9}Ni_{0.1}O_{3\pm\delta}$ sample retained all of its perovskite structure, even after the reduction. In addition, $La_{0.8}Sr_{0.2}Mn_{0.9}Ni_{0.1}O_{3\pm\delta}$ had 1.6% metallic nickel, whereas $LaMn_{0.9}Ni_{0.1}O_{3\pm\delta}$ only had 1.2% metallic nickel, further confirming that the strontium-free composition was thermodynamically more stable and resistant to reduction. The only sample to lose a greater amount of nickel from its perovskite structure was $La_{0.8}Sr_{0.2}Fe_{0.9}Ni_{0.1}O_{3\pm\delta}$, which accommodated the loss of nickel by forming a slightly disordered structure. In the three strontium-free compositions, the amount of nickel lost from the perovskite lattice during reforming correlates well with the thermodynamic stability of the parent (nickel-free) perovskite phase—$LaCr_{0.9}Ni_{0.1}O_{3\pm\delta}$ retained the most nickel in its perovskite lattice, whereas $LaMn_{0.9}Ni_{0.1}O_{3\pm\delta}$ lost the most nickel from its perovskite lattice.

Interestingly, the amount of metallic nickel formed in these samples did not correlate with the differences in the hydrogen yields shown in Figure 4. The worst-performing catalyst at the end of the testing, $LaMn_{0.9}Ni_{0.1}O_{3\pm\delta}$, showed significant coking, as shown in Table 1; apparently, carbon deposition blocked the active sites. The second-lowest-performing catalyst was the $La_{0.8}Sr_{0.2}Fe_{0.9}Ni_{0.1}O_{3\pm\delta}$ sample, which had the highest amount of metallic nickel. The SEM image for this sample, shown in Figure 6a, reveals that the Ni particles were larger than the Ni particles in the analogous Cr and Mn samples shown in Figures 6b and 6c; thus, there was less catalytically active Ni surface area per gram of free nickel in that sample.

5. Conclusions

Samples with compositions of $La_{1-x}Sr_xM_{0.9}Ni_{0.1}O_{3\pm\delta}$ (where M = Cr, Mn, Fe and $x = 0$ or 0.2) were tested for their ability to autothermally reform iso-octane. The chromium-containing compositions had the highest hydrogen yields, and they did not accumulate carbon over 6.5 h of testing. With neutron diffraction, we were able to show that metallic nickel formed in all of the samples during autothermal reforming (ATR). The undoped and strontium-doped Cr- and Fe-based perovskites were tolerant of the loss of nickel, as was the undoped Mn-based perovksite, but the strontium-doped Mn-based perovskite was not. Strontium doping promoted the loss of nickel from the perovskite lattice in all three analogs. The chromium-containing perovskites retained the most nickel in their structures during ATR, because of their inherent resistance to reduction. The catalyst $La_{0.8}Sr_{0.2}Fe_{0.9}Ni_{0.1}O_{3\pm\delta}$ formed the highest amount of free metallic nickel; however, this did not improve the catalytic performance, presumably because of increased sintering of the nickel particles. Five of the six perovskite compositions tested showed no breakdown of the perovskite lattice, despite the loss of nickel from the B-sites—a finding that is surprising because B-site-deficient 3d perovskites are rare.

Acknowledgment. The authors acknowledge Simine Short of the Intense Pulsed Neutron Source at Argonne National Laboratory and Janelle Critchfield, a participant in the Summer Science Undergraduate Laboratory Internship Program sponsored by the Division of Educational Programs at Argonne National Laboratory, for their contribution to this paper. The authors also acknowledge Donald Graczyk, Florence Smith, Susan Lopykinski, Seema Naik, and Lynn TenKate of the Argonne Analytical Chemistry Laboratory for their work on the carbon content determinations and the ICP−OES measurements. The electron microscopy was conducted at the Electron Microscopy Center for Materials Research at Argonne. This work was supported by the U.S. Department of Energy, Office of Energy Efficiency and Renewable Energy, Hydrogen, Fuel Cells, and Infrastructure Technologies Program. The submitted manuscript has been created by UChicago Argonne, LLC, Operator of Argonne National Laboratory ("Argonne"). Argonne, a U.S. Department of Energy Office of Science laboratory, is operated under Contract No. DE-AC02-06CH11357. The U.S. Government retains for itself, and others acting on its behalf, a paid-up nonexclusive, irrevocable worldwide license in said article to reproduce, prepare derivative works, distribute copies to the public, and perform publicly and display publicly, by or on behalf of the Government.